Title

Controlling ERK Activation Dynamics in Mammary Epithelial Cells with Alternating Electric Fields through Microelectrodes.

Journal

Nano letters, 19(10)

ISSN

1530-6984

Authors

Guo, Liang
Li, Houpu
Wang, Yuan
et al.

Publication Date

2019-10-01

DOI

10.1021/acs.nanolett.9b03411

Peer reviewed

Communication

Controlling ERK Activation Dynamics in Mammary Epithelial Cells with Alternating Electric Fields through Microelectrodes

Liang Guo, Houpu Li, Yuan Wang, Zhuo Li, John Albeck, Min Zhao, and Quan Qing

Nano Lett., **Just Accepted Manuscript** • DOI: 10.1021/acs.nanolett.9b03411 • Publication Date (Web): 05 Sep 2019

Controlling ERK Activation Dynamics in Mammary Epithelial Cells with Alternating Electric Fields through Microelectrodes

Liang Guo[1 ‡], Houpu Li[2 ‡], Yuan Wang[2], Zhuo Li[6], John Albeck[3], Min Zhao[1,4,], Quan Qing[2,5,*]*

[1] Department of Dermatology, [3] Department of Molecular and Cellular Biology, [4] Department of Ophthalmology and Vision Science, University of California, Davis, CA, 95616, USA

[2] Department of Physics, [5] Biodesign Institute, Arizona State University, Tempe, Arizona 85287, United States

[6] Key Laboratory of Radar Imaging and Microwave Photonics, Ministry of Education, College of Electronic and Information Engineering, Nanjing University of Aeronautics and Astronautics, Nanjing, 211106, People's Republic of China

Keywords: ERK pathway; EGFR; electric field stimulation; microelectrode;

Abstract:

Amplitude, duration, and frequency of activation of the extracellular-signal-regulated kinase (ERK) pathway code distinct information to instruct cells to migrate, proliferate, or differentiate. Synchronized frequency control of ERK activation would provide a powerful approach to regulate cell behaviors. Here we demonstrated modulation of ERK activities using alternative current (AC) electric fields (EFs) applied through high-k dielectric passivated microelectrodes. Both the amplitude and frequency of ERK activation can be precisely synchronized and modulated. ERK activation in our system is independent of Faradaic currents and electroporation, thus excluding mechanisms of changes in pH, reactive oxygen species and other electro-chemical reaction. Further experiments pinpointed a mechanism of phosphorylation site of epidermal growth factor (EGF) receptor to activate the EGFR-ERK pathway, and independent of EGF. AC EFs thus provide a powerful platform for practical and precise control of EGFR-ERK pathway.

The ERK signaling pathway regulates critical cell behaviors, including, for example cell motility, survival, proliferation and fate determination/differentiation [1-9]. Aberrant signaling of this pathway underlies many important diseases, including cancer and diabetes [10, 11]. How are such diverse consequences coded by ERK activation? Recent advances in imaging the dynamics of ERK activation with single cell resolution have started to reveal critical coding mechanisms and rich information embedded therein. For example, the decision to enter S phase and proliferation of mammary epithelial cells (MCF10A cells) is influenced by the frequency of ERK activation [1]. The change in ERK dynamics in PC12 cells modulated by different pulsed EGF stimulations can decide whether they proliferate or differentiate into neuron-like cells [8, 9]. In addition, the critical roles of ERK activation dynamics *in vivo* have also been demonstrated. In mouse epidermis, upon injury, ERK activation propagates as waves in parallel to the wound edge and is associated with G2/M cell cycle progression [12]. In C. elegans development, Ras-mediated cell fate specification involves different spatiotemporal pulses of ERK activation [13].

A practical method to control the frequency as well as amplitude of ERK activation will be of great value in both basic research as well as possible clinical applications. Frequency modulation (FM) of ERK activation has been achieved with optogenetics, where genetically modified light sensitive molecules are expressed in target cells and light signals are shined at controlled frequency upon cells [14]. Another method of FM is through pulsed stimulation with EGF (epidermal growth factor), in which addition and washout of EGF is repeated at required frequency [8, 15].

We report here a method of frequency modulation of ERK activation that does not require repeated addition and washout of chemicals, or genetic-modification of cells. We used an alternating current (AC) electric field (EF) stimulation to induce defined FM of ERK activation.

We show that time-modulated symmetric bipolar AC EF of tens of kHz can directly trigger highly localized and synchronized ERK activation without Faradaic process. We provide evidence for selective AC EF induced ligand-independent EGFR phosphorylation. Our work suggests a new strategy and practical technology of precise ERK modulation with high spatial resolution and temporal control, and may have significant implications for design of electroceuticals to regulate important biological processes and treat diverse diseases through FM of intracellular signaling pathways.

Firstly, we briefly introduce the ERK activation reporter used in our experiment and the design of the microelectrode chip. ERK translocation reporter (ERKTR) can be used to report activation dynamics of ERK in a spontaneously immortalized mammary epithelial cell line (MCF10A) [16, 17]. Upon activation of EGFR-Ras-ERK pathway, the mCherry-labelled ERKTR is phosphorylated and translocated from the nucleus to the cytosol, causing fluorescence intensity decrease in the nucleus region and increase in the cytosol (Fig. 1a). The ratio of fluorescence intensity in the cytosol (Fc) and that in the nucleus (Fn), i.e., ERKTR ratio, thus gives a quantitative *in situ* assessment of ERK activation of an individual cell with high temporal resolution (see Supplementary Information, *Materials and Methods*). With this real-time reporting system, we ask two questions: (1) How precisely in space and in time can we control ERK activation with EF? (2) What is the possible mechanism that EF couples with the ERK signaling pathways?

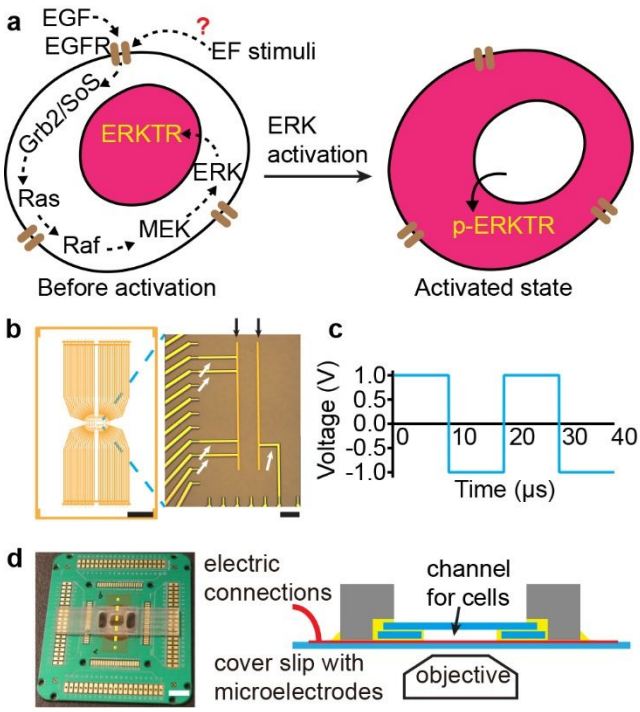

Figure 1. The reporter cell and chip design. (a) A schematic of ERK translocation reporter (ERKTR, pink color) translocate from the nucleus to cytosol upon activation of EGFR-Ras-ERK signaling pathway. (b) Left: The overall of the microelectrode arrays on the glass cover slip. Right: An optical image of one pair of microelectrodes at the center of the chip. The white arrows mark the metal connections that are passivated by 500 nm thick SU-8 polymer. The black arrows mark the exposed parallel microelectrodes. Scale bars, left: 5 mm, right: 200 μm. (c) The waveform of the bipolar electric pulses applied to the electrodes. (d) Left: A photo of the assembled cell chamber on the chip and printed circuit board (PCB). Scale bar 10 mm. The yellow dash line marks the position of the cross-section shown on the right. Right: Schematics of the cross-section structure of the chamber.

To address these questions, we prepared customized microelectrode chips to deliver local EF to the cells with several key considerations. First, a pair of microelectrodes were used to interface with the cells so that the EF was localized close to the electrodes and decayed rapidly outside the vicinity. The electrodes were fabricated by top-down lithography on a 170 μm thick glass cover slip. The metal connections were passivated by a layer of SU-8 epoxy by photolithography, leaving only the parallel electrode bars exposed, which had an edge-to-edge distance ranging between 50 to 200 μm (Fig. 1b). Second, bipolar symmetrical electric pulses were used in our

experiments to eliminate net direct current (DC) ionic flows in the system. Specifically, due to the small exposed surface area of the electrodes, the electric signals were coupled to the medium capacitively as through a high-pass filter with an impedance of ~120 Ω at 50 kHz (See SI Appendix). The designed signal has fast rising and falling edges and a width of 10 μs to enhance the potential drop within the medium (Fig. 1c). Third, the electrodes and circuits connected to them were isolated from all other grounds. We have performed cyclovoltammetry on these electrodes in the assay medium and there was no significant redox current in a slow voltage sweep between -1.0 V and 1.0 V (See Supplementary Fig. S1a). In addition, the stability of the electrodes was tested with prolonged application of up to ±1.5 V bipolar pulses for >1 hour and no degradation of the metal surface was observed (See Supplementary Fig. S1b). The simulation of the EF distribution (COMSOL Multiphysics, see Supplementary Information, Materials and Methods) showed that when an AC (1 V, 50 kHz) was applied between a pair of metal electrodes 200 μm apart in homogeneous medium, the EF strength close to the surface of the substrate and at the center of the electrode pair was ~8 V/cm, and close to the edge of the electrode ~24 V/cm (See Supplementary Fig. S2). Last, the chip was assembled into an observation chamber with a thin fluidic channel over the electrode arrays (W 0.5 cm × L 1.0 cm × H 170 μm) where cells were plated and cultured. After wire bonding, the chamber can be mounted on an inverted microscope for imaging as EF stimuli were applied (Fig. 1d) (see Supplementary Information, Materials and Methods).

Secondly, we studied the localized activation of ERK by AC EFs on our platform. About 3-6 minutes after onset of stimulation, fluorescence intensity of the nuclei started to decrease and fluorescence intensity of cytosol increase, indicating ERK activation. Fig. 2a is a typical image took at 9 min after the EF stimuli delivery. The majority of cells close to the electrodes

demonstrated clear ERK activation (Fig. 2b). Cells more than 200 μm away from the electrode region remained silent, including those that were close to the SU-8 passivated connections (Fig. 2c).

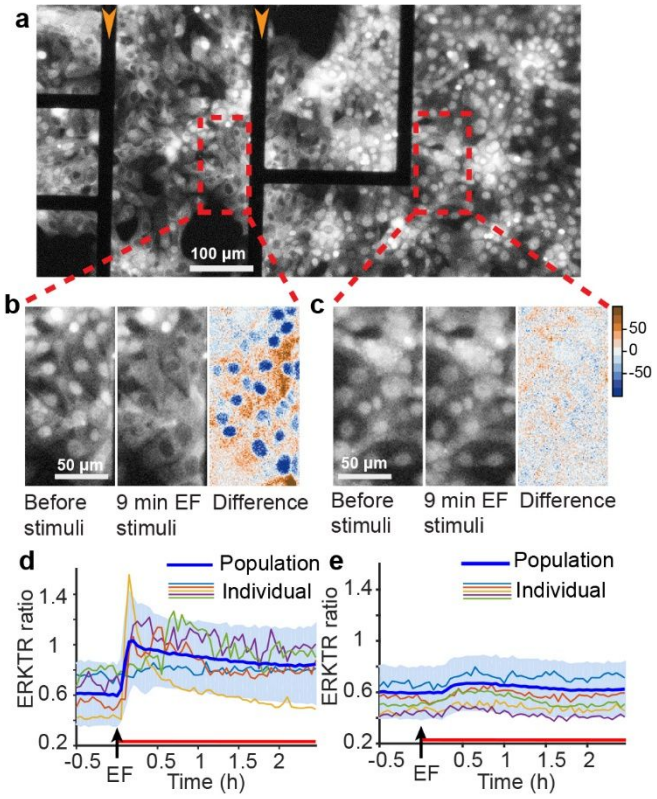

Figure 2. Localized ERK activation by AC EF. (a) AC EF induced localized ERK activation between a pair of microelectrode bars (marked by the arrows). (b-c) Cells between the microelectrodes (b) and in an adjacent area (c) before and after onset of stimulation. The color-coded images on the right of each panel show the difference of fluorescence intensity before and after stimulation. Blue and orange colors mark areas where the fluorescence intensity decrease and increase respectively. (d) Time traces of ERKTR ratio of individual representative cells and population average from 164 cells within 100 μm from the electrode. Average data are presented as mean (thick blue line) ± SD (light shadow). Black arrow denotes the time of applying AC-EF and red line indicate the sustained EF stimuli. (e) Time traces of ERKTR ratio of individual representative cells and population average from 160 cells within the region of 200 to 700 μm away from the electrode. Data are presented as mean (thick blue line) ± SD (light shadow). Black arrow denotes the time of applying AC-EF and red line indicate the sustained EF stimuli.

ERK activation indicated by the ERKTR ratio (Fc/Fn) demonstrated synchronized initial response with heterogeneous dynamics for cells resided within 100 μm from the electrodes. Before onset of EFs, only very few displaying limited low-level spontaneous ERK activity. About 9 minutes after onset of the stimulation, cells showed ERK activation with different amplitude and duration (Fig. 2d). Majority of the cells showed response between 6 min to 18 min following onset of the stimulation. Under continuous EF exposure, the ERK activation level of the majority of cell population gradually decreased towards the baseline in 29 ± 13 minutes. Cells that are far away from the open electrode area showed no ERK activation by EF (Fig. 2e). The heat maps summarizing the ERK activation in both areas are given in Supplementary Fig. S3.

We note that activation of ERK is highly localized: more than 80% of cells within the range of 50 μm from the electrodes showed clear ERK activation, and the ratio decreased rapidly to below 20% as the distance increased to more than ~100 μm. Very few cells showed ERK activities 300 μm away from microelectrodes (See Supplementary Fig. S4). In addition, under extended EF stimulation, oscillatory patterns in the ERK level could be observed for a small portion of the cells (Fig. 3a, b). The peaks and valleys of all the ERKTR ratio time traces were identified using a threshold method automatically (see Supplementary Information, Materials and Methods). About 20% of cells showed ERK activation cycle twice or more (Fig. 3c).

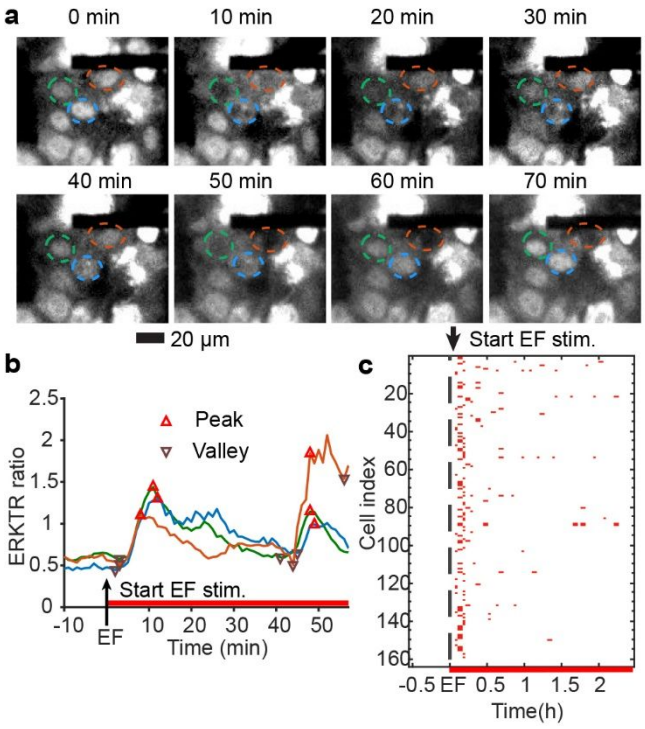

Figure 3. ERK oscillations under sustained AC EF stimulation. (a) Three cells showing oscillation of ERK under continuous AC EF stimulation. Fluorescent images taken at 0, 10, 20, 30, 40, 50 and 60 minute as continuous AC EF stimuli were applied. Cells circled in orange, blue, and green all demonstrated repeated pulsatile ERK activation. Scale bar: 20 μm. (b) Time traces of the ERKTR ratio of the three cells in (a), peaks (ERK active) and valleys (ERK at rest) were identified. The black arrow denotes the start time of EF stimulation and red line marks the sustained EF stimuli. (c) Peak time map of the 164 cells in Fig. 2D under sustained AC EF stimulation. 35 cells showed multiple peaks (>=2) in 3 hours. The black dashed line indicated the time of exposure to AC EF stimulation.

Thirdly, we show that no Faradaic process or electroporation were involved in the AC EF activation of ERK, and neither Ca^{2+} nor reactive oxygen species (ROS) mediated this process. To exclude the possibility of ERK activation related to cell damage [18], we investigated the possibility of cell membrane damage using membrane impermeable dyes. Sytox orange (50 μM, Invitrogen) which stains the nucleus and cannot penetrate intact cell membrane, was added in the medium, and AC EF stimulation was continuously applied for >1 hour. Except for very few cells that were

in direct contact with the metal electrodes, almost all the cells remained unstained, suggesting no membrane damage (See Supplementary Fig. S5a, b). In addition, cells were stained using the Cell Viability Imaging Kit (Cat#R37609, Life Technologies, see Supplementary Information, Materials and Methods), 2 hours after confirming the reproducible ERK activation. More than 95% of the cells remained alive and healthy after the experiment. We also calculated the proliferation rate of cells 24 hours after confirming EF activation of ERK as 1.26 ± 0.11, which has no significant difference to the ratio 1.22 ± 0.14 obtained from control groups (See Supplementary Information, Materials and Methods, Fig. S6).

To exclude any electrochemical reactions that could interfere with the EF activation of ERK, we added an extra layer of high-k passivation layer over the terminal electrode surface, which blocks all redox reactions while not increasing the impedance of the electrodes significantly (See *Supplementary Information Text*, Supplementary Fig. S7a, b). Specifically, we deposited over the entire surface of the chip 10 nm HfO_2 by atomic layer deposition (ALD). Cyclic voltammetry test (see Supplementary Information, Materials and Methods) confirmed that the HfO_2 coating completely suppress the Faradaic process (see Supplementary Fig. S7c). Our impedance analysis shows that the capacitive impedance of the added HfO_2 layer at 50 kHz is about 7 kΩ, which is comparable to the resistance of the medium layer between the electrodes (See SI Appendix). With this new design of passivated electrodes, we showed that ERK can still be reliably activated by EF stimuli (see Supplementary Fig. S7d), with an expected higher threshold pulse amplitude (typically between 1.5V~3V) due to the increase of the impedance. In addition, we have confirmed that neither Ca^{2+} chelator (BAPTA AM, 3 μM, Life Technologies), nor ROS quencher (Trolox, 350 μM, Sigma-Aldrich) could block the EF activation of ERK (See Supplementary Fig. S8), which also suggests that ERK activation in our system is unlikely mediated by Ca^{2+} changes

or ROS, contrary to previously suggested mechanism when DC EF stimulations were applied [19, 20]. The observed activation of the ERK thus was not associated with redox processes at the electrode interface.

Fourthly, we demonstrate that no local temperature increase or diffusion limited process were involved in the activation or ERK. We measured the local temperature by tracking the current of a patch clamp pipette electrode before and after the application of AC EF[21]. A patch clamp pipette freshly prepared by a micropipette puller (P-1000, Sutter Instruments, see Supplementary Information, Materials and Methods) was filled with 0.1 M KCl, giving a typical resistance of 7-10MΩ. The tip of the patch clamp pipette was positioned within 10 μm above the substrate between the electrodes in a clean chamber by a micromanipulator (MP-225, Sutter Instruments), using Ag/AgCl sealed in 0.1M KCl as the reference electrode through a salt gel bridge. The room temperature was regulated at 21.6±0.2 °C. A bias of 10 mV was applied to the pipette electrode as the current was monitored through a patch clamp amplifier (HEKA EPC 800 USB). Since the current will be sensitive to the local temperature at the very opening of the pipette, we can use the current to evaluate the local temperature changes. Ten groups of measurements were performed for 3 and 10 minutes of AC EF stimulations each. When bare Au microelectrodes were used, the calculated temperature change was 0.00 ±0.05 °C and 0.01±0.07 °C respectively, and 0.03±0.07 °C and 0.01±0.05 °C respectively when HfO_2 coated microelectrodes were used (See Supplementary Fig. S9). Therefore, we conclude that there was no appreciable local temperature increase due to the application of AC EF stimulations in our setup in the course of the ERK activation. In addition, we exposed the MCF10A cells to different temperatures between 35 °C and 39 °C, and the spontaneous ERK activities were most active between 35 °C to 37 °C. Cells demonstrated much reduced spontaneous ERK activities at higher temperature (See

Supplementary Fig. S10). These data suggest that local temperature increase was not involved in the observed ERK activation.

In addition, we have studied the onset time of the ERK response for cells at different distances (0-100 μm) from the electrodes. Cells have overall shown clear timing variations in their responses such that the onset time of the ERK activation scattered in a wide range from 6 minutes up to 36 minutes (See Supplementary Fig. S11). Interestingly, more than 79% cells (n=216) were activated within 15 minutes independent of where they were, which strongly suggested a direct interaction with the AC EF. On the other hand, < 21% of the cells, all of which were >25 μm away from the electrodes, showed 18-36 minutes onset time that appeared rather randomly distributed, which could be attributed either to spontaneous activities, or a diffusion-related process, for example, intercellular communications. In addition, if Joule heating related process were involved, since the current density was higher where it was closer to the electrodes, more pronounced temperature changes would happen faster near the electrodes and slower at farther distance, which was not observed from the onset time distribution. Therefore, this result also suggested that temperature change was not an important factor.

Fifthly, we demonstrate that the ERK activation can be precisely synchronized and modulated by AC EFs. Given the localization and synchronized onset of the ERK activation by AC EF, it is therefore possible to control the frequency of the ERK activation for a selected population of cells simply by cycling AC EF on and off with the right timing. As an example, we have achieved very robustly synchronized and enhanced ERK activation at a rate of about twice per hour. Specifically, in one cycle, a 3 min train of bipolar pulses was delivered to the electrodes, during which time no cell response generally has started to appear yet, followed by a ~40 min period in which the EF is turned off. This cycle was repeated for three times in the experiment (See

Supplementary Fig. S12). Three activation events are readily observed 3-6 minutes following the AC EF stimuli at 0 minute, 48 minute, and again 93 minute as shown in Fig. 4a. The time traces of the ERKTR ratio showed three distinct activation peaks (Fig. 4b), which are also evident in the heat map plot (See Supplementary Fig. S13) and peak time map (Fig. 4c). We noticed that if the duration of EF stimulation in each cycle is reduced shorter than 3 min, we observed less reproducible ERK activation in much fewer cells. In addition, since the time interval of our image sequence is currently limited to 3 minutes, the selected snapshots might not capture the maximum response of all cells.

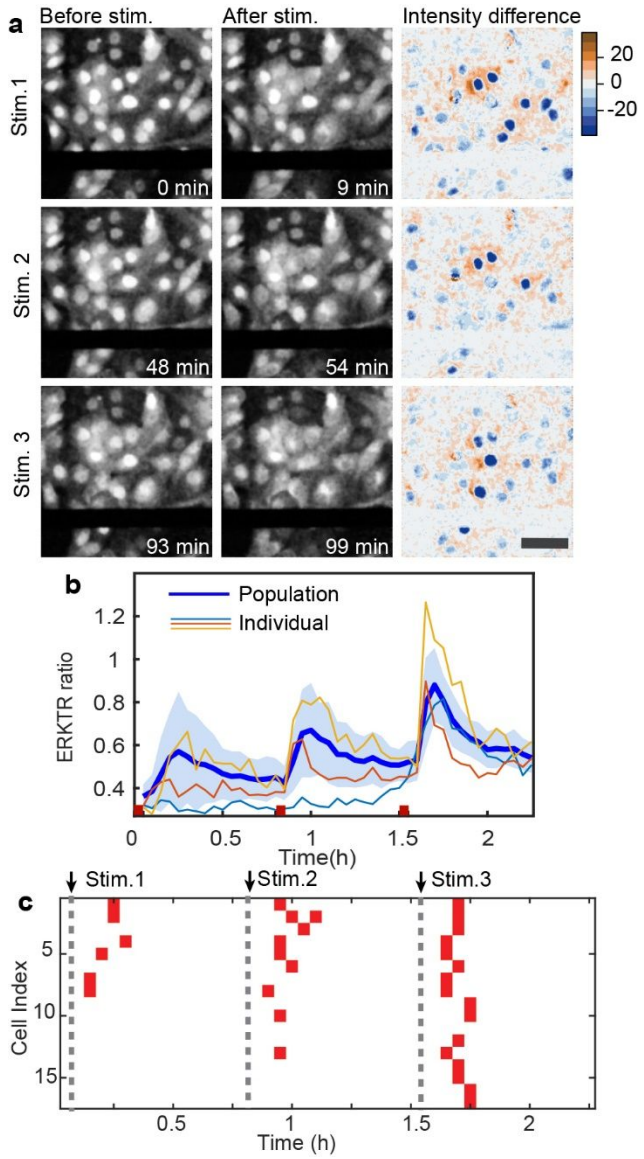

Figure 4. Repeated short AC-EF stimulation induced synchronized ERK activation. (a) Fluorescent images of cells before (left) and after (middle) the 3-minute long AC EF stimulations started at 0, 48 and 93 min. Right: Color coded intensity difference. Blue and orange colors mark areas where the fluorescence intensity decreased and increased, respectively. Scale bar: 50 μm. (b) Time traces of ERKTR ratio from individual representative cells and population average from 17 cells. The short red lines mark the duration of EF stimuli. Data are presented as mean (thick blue line) ± SD (light shadow). (c) Peak time map of ERK activities.

From Fig. 4, we can see that ~50% of the cells within 100 μm range from the electrodes showed repeated ERK activation by all three short stimulations, while ~30% cells started responding either after the second or the third one. All cells restored to its low ERK level state within an average time of 15 ± 6 minutes. Interestingly, later stimulation induced more cells to respond in a synchronized manner. These results show that we can precisely synchronize the ERK activation with specific frequency by a minimal duration of localized AC EF stimulation.

Lastly, we show that the phosphorylation site of EGFR is the target of ACEF to activate ERK. Since we can exclude the involvement of electroporation, pH change, ROS and Ca^{2+}, and temperature fluctuations, how did AC EF induce the ERK activation? To determine the detailed mechanism, we systematically inhibited various elements of EGFR-ERK signaling pathway. The canonical EGF-Ras-ERK signaling pathway is initialized by the binding of EGF to the EGFR, which triggers the dimerization and phosphorylation of EGFR, leading to Raf-MEK-ERK signaling (Fig. 5a) [22, 23]. We first applied the MEK inhibitor, trametinib (0.5 μM, Selleck Biochemicals), to the cells when trying to activate ERK using either AC EF (Fig. 5c, left columns) or with EGF as comparison (Fig. 5c, right column). In both cases, we observed inhibition of the ERK activation. Similarly, the Raf inhibitor, sorafenib (20 μM, Biotang) also abolished ERK activation under both stimulation scenarios (Fig. 5d). In addition, several small molecule tyrosine kinase inhibitors (TKIs) that binds to the intracellular tyrosine kinase domain of the epidermal growth factor receptor family (ErbB) family of receptors, including the irreversible pan-ErbB inhibitor, afatinib (5 μM, Selleck Biochemicals), which covalently binds to EGFR, HER2 and HER4 [24], and the reversible EGFR selective inhibitors, erlotinib (2 μM, Selleckchem), and gefitinib (50 μM, Selleckchem) [24], was tested respectively. In all cases, the ERK activities were silenced under EF stimulation (Fig. 5e-g, respectively). Surprisingly, however, when EGFR

antibody cetuximab (100 μg/mL, ERBITUX) was used just to block the extracellular EGF binding site to the EGFR but leave the phosphorylation site intact, the AC EF could still activate ERK, although with an overall reduced contrast in the fluorescent signals (Fig. 5h). These were in sharp contrast to the tests with EGF stimulation controls where both TKIs and EGF antibody blocked ERK activation by EGF stimulations (control groups in Fig. 5b-h). The time evolution of the ERKTR ratios in all blocker tests under EF stimulation are summarized in Fig. 5i, where we can see that the only trace showing ERK activation other than the blank control was the case where EGFR antibody were applied. We also note that for EGF antibody tests, a small retardation in time was often observed. The heat maps of the ERKTR ratio from all recorded cells are summarized in Supplementary Fig. S14. These results strongly suggest that the coupling between EF and ERK specifically followed the EGFR-Ras-ERK signaling pathway, initialized by EF-induced EGF-independent kinase activity of EGFR.

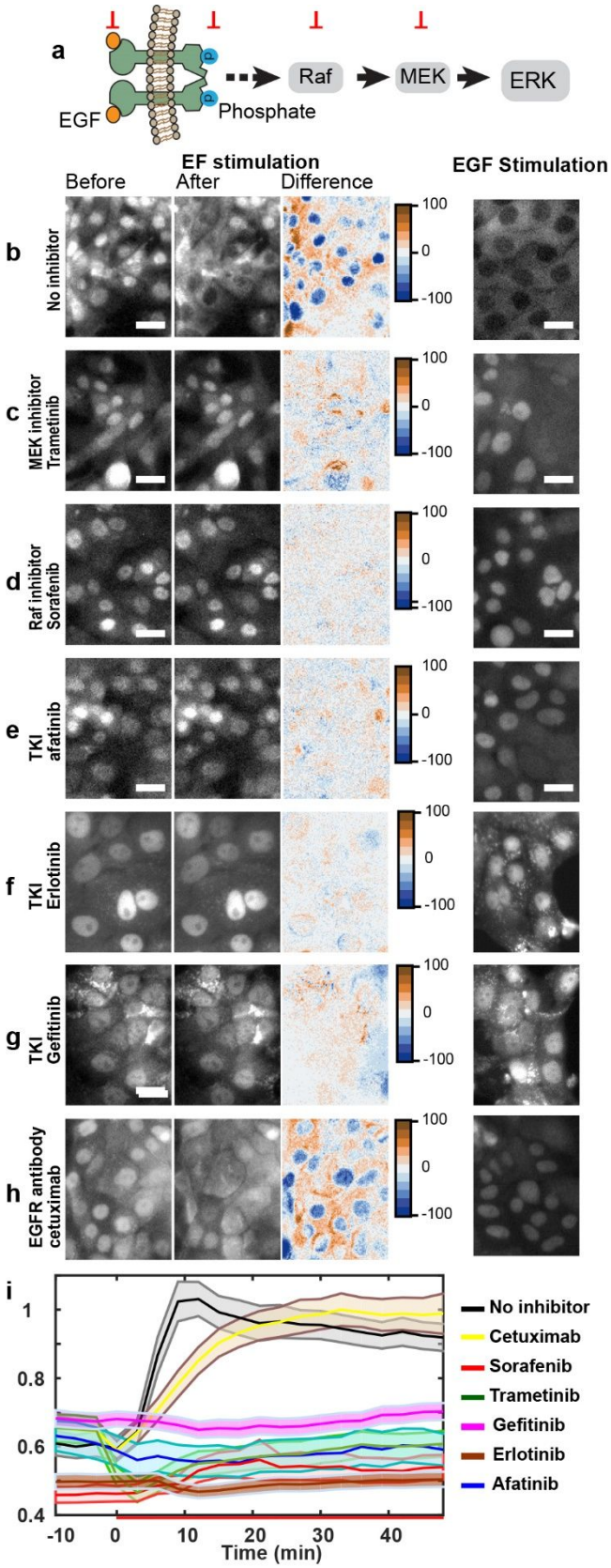
a
EGF
Phosphate
Raf
MEK
ERK
EF stimulation
EGF Stimulation
Before
After
Difference
b No inhibitor
c MEK inhibitor Trametinib
d Raf inhibitor Sorafenib
e TKI afatinib
f TKI Erlotinib
g TKI Gefitinib
h EGFR antibody cetuximab
100
0
-100
i
1
0.8
0.6
0.4
-10
0
10
20
30
40
Time (min)
No inhibitor
Cetuximab
Sorafenib
Trametinib
Gefitinib
Erlotinib
Afatinib

Figure 5. Blocker tests following the EGFR-Raf-ERK signaling pathway. (a) Schematics of the EGF-Ras-ERK signaling pathway and the blocked sites, including the extracellular EGF binding site, the intracellular phosphorylation site of EGFR, Raf and MEK. (b-h) (Images on the left group) Fluorescence images of cells before and after AC EF stimulation, and the intensity difference; and (Images on the right group) fluorescence images of control groups stimulated by EGF chemical stimulation (2ng/mL), when no inhibitors were applied (b), and with MEK inhibitor trametinib (0.5 μM) (c), Raf inhibitor sorafenib (20 μM) (d), tyrosine kinase inhibitors afatinib (5 μM) (e), erlotinib (2 μM) (f), gefitinib (50 μM) (g), and EGFR binding-site antibody cetuximab (100 μg/mL) (h), respectively. Scale bars: 25 μm. (i) Time traces of ERKTR ratio as population average from cells under AC EF stimulations in (b-h). Mean and ± 95%CI are shown as a solid line and shadow region, respectively (n > 100 cells for each group).

Precise modulations of the magnitude and the frequency/duration of ERK activity are fundamentally significant as both can impact the physiological outcome of ERK signaling in subtle, yet critical ways [1, 8, 25, 26]. Compared to chemical methods that usually have poor control in temporal and spatial resolution, our result of AC EF activation of ERK has its unique advantages as the spatial distribution and timing of EF can be engineered to accurately localize and synchronize events at the single-cell level. We have shown that AC EF can induce synchronized ERK activation under continuous stimulation (Figs. 2 and 3), and more importantly, provide precise control of ERK dynamics (Fig. 4). It is therefore possible to accurately modulate the location, time, frequency, amplitude and duration of ERK activities by localized AC EF, without the requirement of genetic manipulation as in the case of optogenetics [14], or addition and washout of chemicals [8].

To date, investigations on how external EF couples with the ERK signaling pathways have all been focused either on direct-current (DC) and low frequency EF (several hundred Hz), or fast nanosecond pulses and high frequency radiations (several GHz). For example, Wolf-Goldberg et al showed that low frequency unipolar EF pulses (~500Hz) applied through bare Pt electrodes in solution can cause ligand-independent activation of epidermal growth factor (EGF) receptor

(EGFR), leading to ERK activation [19], where the pH changes and ROS due to electrochemical process at the electrode interface were identified as the possible cause. In addition, nanosecond pulses have been shown to activate p38, c-Jun N-terminal kinase (JNK) and ERK signaling pathways [27, 28], which was attributed to cell membrane electroporation and cytosolic Ca^{2+} level changes due to the EF stimulation. Furthermore, Sheikh et al. showed that microvascular endothelial cells that were exposed to 24 hours of high frequency EF (7.5 GHz) demonstrated enhanced ERK phosphorylation, among several other processes, where cRaf/MEK and Ca^{2+} pathways were involved.

Several major differences between our study and existing approaches should be highlighted. First, we used bipolar symmetric EF pulses with high-k dielectric passivated electrodes designed to eliminate Faradaic processes. This avoids possible biochemical complications and possible detrimental effects known that can happen to living cells and tissues with other techniques, where DC, unipolar or asymmetric EF were typically coupled to the cells through a low impedance metal interface in direct contact with the medium. We have, for the first time, clarified that intermediate ion flows and chemical species generated by electrochemical processes are not required for EF coupling with ERK signaling pathway. Second, no strong perturbation of the cell integrity was observed in our experiments (see Supplementary Information, Materials and Methods) due to the low EF strength, and the main frequency component of the EF (~50 kHz) falls in a middle range that has not been investigated before. Third, we have identified that AC EF can induce EGF-independent phosphorylation of EGFR which triggers the ERK signaling pathway. Although ligand-independent EGFR phosphorylation has been observed previously with bias applied through low-impedance Pt electrodes in contact with the medium, where ROS and

decrease in pH were found to be the cause [19], however, here we have shown that no electrochemical processes are involved in our study.

Using oscillating EF to tune membrane protein activities has been studied in Na-K pumps systems [29]. Specifically, it has been shown that when the frequency of the external EF matches the natural pumping rates of Na-K pumps (~50 Hz), individual pumps with initially different pumping rates and random pumping phases can be synchronized to generate enhanced transepithelial potential (TEP), due to field-induced energy changes in the ion-transports. However, in our case, the EGFR is not electrogenic and should not be sensitive to ion gradients, and the time scale of the EF pulses (10-20 μs) is obviously much faster in comparison to the operation time of ion pumps. More importantly, the comparison between AC-EF induced and EGF-induced ERK activation in our blocker tests (Fig. 5) revealed an intriguing difference, that the extracellular EGFR antibody could only block the EGF stimulation but not the AC EF. This indicates that the AC EF could directly induce the EGFR phosphorylation without requiring EGF binding. To our knowledge, those results are the first demonstration of such unusual possibility, in addition to cases where EGFR can be "transactivated" through ligands binding to other receptors [30]. Our data suggest that there could be a new type of direct interaction between AC EF in this frequency range and membrane proteins such as EGFR. A possible explanation is that the spatial distribution of AC EF can be concentrated across the membrane of live cells in a frequency-dependent manner, which could modulate electrostatic interactions at the right time scale in favor of functional conformation changes of proteins [31]. We estimated the transient transmembrane voltage during one half phase of the AC EF to be between 0.1-16 mV (See Supplementary Fig. S15), which is consistent with the calculations by Taghian etc. [32]. While this might potentially bring physiological response from the cells, we note that our AC EF is completely symmetrical around 0 V with very fast switching

time of 20 μs. And the whole process of AC EF activation of ERK signaling pathways is as short as 3-20 minutes. It is unlikely that what we observe is a response to membrane potential, which typically happens in a much longer time scale [33]. In addition, we have not observed appreciable difference in terms of threshold and timing of ERK response to the AC EF stimulation for low density of cells where individual cells are not in contact with each other (See Supplementary Fig. S16). Therefore, we suggest the observed ERK activation is more likely to be related to a rather fast dynamic process at the cell membrane induced by the AC EF. The detailed molecular mechanism of the specific phosphorylation of EGFR by external AC EF as first demonstrated here still need further investigation and modeling.

In summary, we have demonstrated non-invasive and highly localized technique to precisely control ERK activation dynamics by bipolar AC EF pulses applied through microelectrodes with no Faradaic processes involved. ERK activity in multiple cells can be reproducibly synchronized and modulated in time. The ERK activation seemed to be specifically initiated by EF induced EGF-independent phosphorylation of EGFR, and does not involve changes in pH, Ca^{2+} or ROS. Our work can serve as a unique platform for precise modulation of ERK activities and possibly other signaling pathways, and can find wide biomedical applications to control cell behaviors through modulating signaling dynamics which is difficult to achieve otherwise.

Methods

MCF10A cells co-express ERKAR3 and ERKTR-mCherry [17] were cultured in customized chamber with microelectrode arrays fabricated on the bottom cover slip for EF stimulation during imaging. The cells were starved for 2 hrs in EGF-free medium before experiments. AC EF was generated by a NI 9269 module from National Instruments as the cells were imaged on an

inverted microscope with an incubator chamber. Data processing and statistics were performed using Matlab (MathWorks) and Igor Pro (WaveMetrics). Detailed experiment materials and methods are provided in Supplementary Information.

ASSOCIATED CONTENT

Supporting Information.

The following files are available free of charge.

Supporting Information that includes details on estimation of impedance of microelectrode; Estimation of cross-membrane potential at different AC EF frequencies; materials and methods, supportive figures on cell behavior image and analysis. (PDF)

Movie S1. ERK activity of cells within 100 μm from the electrode response to 1V 50Hz AC EF.

Movie S2. ERK activity of cells more than 200 μm from the electrode response to 1V 50Hz AC EF.

Movie S3. Repetitive 3-minute EF stimulations showing synchronized ERK activation.

Movie S4. Fluorescence images of ERK activation triggered by AC EF from control group of no inhibitor, and from cells with MEK inhibitor, Raf inhibitor, EGFR inhibitor blocking phosphorylation site, and EGFR antibody blocking EGF bind, respectively.

AUTHOR INFORMATION

Corresponding Author

*Correspondence and requests for materials should be addressed to M.Z. (email minzhao@ucdavis.edu) and Q.Q. (email: quan.qing@asu.edu)

Author Contributions

The manuscript was written through contributions of all authors. L.G., H.L, and Y.W. performed research; J.A. provided the cell line used in the research; L.G., H.L., M.Z. and Q.Q. designed research; L.G., H.L., Y.W., M.Z. and Q.Q. analyzed data; Y.W. and Z.L. performed impedance analysis and simulation of EF distribution; L.G., H.L., M.Z. and Q.Q. wrote the paper. All authors have given approval to the final version of the manuscript.

‡ Liang Guo and Houpu Li contributed equally.

Funding Sources

Air Force Office of Scientific Research under award number FA9550-16-1-0052

the National Institute of Biomedical Imaging and Bioengineering of the National Institutes of Health under award number R21EB020822

National Institute of Biomedical Imaging and Bioengineering of the National Institutes of Health under award number R21EB015737 and NIH R01EY019101

Notes

ACKNOWLEDGMENT

Q.Q. and M.Z. acknowledge the support by the Air Force Office of Scientific Research under award number FA9550-16-1-0052. Q.Q. acknowledges the support by the National Institute of Biomedical Imaging and Bioengineering of the National Institutes of Health under award number R21EB020822, M.Z. acknowledges the support by the National Institute of Biomedical Imaging and Bioengineering of the National Institutes of Health under award number R21EB015737 and NIH R01EY019101. The content is solely the responsibility of the authors and does not necessarily represent the official views of the National Institutes of Health.

ABBREVIATIONS

ERK, extracellular-signal-regulated kinase; AC, alternative current ; EF, electric field; EGF, epidermal growth factor ; FM, Frequency modulation ; ERKTR, ERK translocation reporter ; DC, direct current ; ROS, reactive oxygen species ; TKI, tyrosine kinase inhibitor; JNK, c-Jun N-terminal kinase ; TEP, transepithelial potential

REFERENCES

1. Albeck, J. G.; Mills, G. B.; Brugge, J. S. *Mol Cell* **2013,** 49, (2), 249-61.
2. Luciano, F.; Jacquel, A.; Colosetti, P.; Herrant, M.; Cagnol, S.; Pages, G.; Auberger, P. *Oncogene* **2003,** 22, (43), 6785-93.
3. Allan, L. A.; Morrice, N.; Brady, S.; Magee, G.; Pathak, S.; Clarke, P. R. *Nature cell biology* **2003,** 5, (7), 647-54.
4. Klemke, R. L.; Cai, S.; Giannini, A. L.; Gallagher, P. J.; de Lanerolle, P.; Cheresh, D. A. *J Cell Biol* **1997,** 137, (2), 481-92.
5. Lai, C. F.; Chaudhary, L.; Fausto, A.; Halstead, L. R.; Ory, D. S.; Avioli, L. V.; Cheng, S. L. *J Biol Chem* **2001,** 276, (17), 14443-50.
6. Roux, P. P.; Blenis, J. *Microbiol Mol Biol Rev* **2004,** 68, (2), 320-44.
7. Wortzel, I.; Seger, R. *Genes Cancer* **2011,** 2, (3), 195-209.
8. Ryu, H.; Chung, M.; Dobrzynski, M.; Fey, D.; Blum, Y.; Lee, S. S.; Peter, M.; Kholodenko, B. N.; Jeon, N. L.; Pertz, O. *Mol Syst Biol* **2015,** 11, (11), 838.
9. von Kriegsheim, A.; Baiocchi, D.; Birtwistle, M.; Sumpton, D.; Bienvenut, W.; Morrice, N.; Yamada, K.; Lamond, A.; Kalna, G.; Orton, R.; Gilbert, D.; Kolch, W. *Nature cell biology* **2009,** 11, (12), 1458-64.
10. Lu, H.; Liu, S.; Zhang, G.; Bin, W.; Zhu, Y.; Frederick, D. T.; Hu, Y.; Zhong, W.; Randell, S.; Sadek, N.; Zhang, W.; Chen, G.; Cheng, C.; Zeng, J.; Wu, L. W.; Zhang, J.; Liu, X.; Xu, W.; Krepler, C.; Sproesser, K.; Xiao, M.; Miao, B.; Liu, J.; Song, C. D.; Liu, J. Y.; Karakousis, G. C.; Schuchter, L. M.; Lu, Y.; Mills, G.; Cong, Y.; Chernoff, J.; Guo, J.; Boland, G. M.; Sullivan, R. J.; Wei, Z.; Field, J.; Amaravadi, R. K.; Flaherty, K. T.; Herlyn, M.; Xu, X.; Guo, W. *Nature* **2017,** 550, (7674), 133-136.
11. Banks, A. S.; McAllister, F. E.; Camporez, J. P. G.; Zushin, P. J. H.; Jurczak, M. J.; Laznik-Bogoslavski, D.; Shulman, G. I.; Gygi, S. P.; Spiegelman, B. M. *Nature* **2015,** 517, (7534), 391-U581.
12. Hiratsuka, T.; Fujita, Y.; Naoki, H.; Aoki, K.; Kamioka, Y.; Matsuda, M. *Elife* **2015,** 4, e05178.
13. de la Cova, C.; Townley, R.; Regot, S.; Greenwald, I. *Dev Cell* **2017,** 42, (5), 542-553 e4.
14. Toettcher, J. E.; Weiner, O. D.; Lim, W. A. *Cell* **2013,** 155, (6), 1422-34.
15. Shankaran, H.; Ippolito, D. L.; Chrisler, W. B.; Resat, H.; Bollinger, N.; Opresko, L. K.; Wiley, H. S. *Mol Syst Biol* **2009,** 5, 332.
16. Regot, S.; Hughey, J. J.; Bajar, B. T.; Carrasco, S.; Covert, M. W. *Cell* **2014,** 157, (7), 1724-34.
17. Sparta, B.; Pargett, M.; Minguet, M.; Distor, K.; Bell, G.; Albeck, J. G. *J Biol Chem* **2015,** 290, (41), 24784-92.
18. Subramaniam, S.; Zirrgiebel, U.; von Bohlen Und Halbach, O.; Strelau, J.; Laliberte, C.; Kaplan, D. R.; Unsicker, K. *J Cell Biol* **2004,** 165, (3), 357-69.
19. Wolf-Goldberg, T.; Barbul, A.; Ben-Dov, N.; Korenstein, R. *Biochim Biophys Acta* **2013,** 1833, (6), 1396-408.
20. Jura, N.; Endres, N. F.; Engel, K.; Deindl, S.; Das, R.; Lamers, M. H.; Wemmer, D. E.; Zhang, X.; Kuriyan, J. *Cell* **2009,** 137, (7), 1293-307.
21. Yao, J.; Liu, B.; Qin, F. *Biophys J* **2009,** 96, (9), 3611-9.
22. McKay, M. M.; Morrison, D. K. *Oncogene* **2007,** 26, (22), 3113-21.
23. Oda, K.; Matsuoka, Y.; Funahashi, A.; Kitano, H. *Mol Syst Biol* **2005,** 1, 2005 0010.
24. Modjtahedi, H.; Cho, B. C.; Michel, M. C.; Solca, F. *Naunyn Schmiedebergs Arch Pharmacol* **2014,** 387, (6), 505-21.
25. Stork, P. J. *Cell Cycle* **2002,** 1, (5), 315-7.
26. Murphy, L. O.; Smith, S.; Chen, R. H.; Fingar, D. C.; Blenis, J. *Nature cell biology* **2002,** 4, (8), 556-64.
27. Morotomi-Yano, K.; Akiyama, H.; Yano, K. *Arch Biochem Biophys* **2011,** 515, (1-2), 99-106.
28. Semenov, I.; Xiao, S.; Pakhomov, A. G. *Biochim Biophys Acta* **2013,** 1828, (3), 981-9.
29. Clausell, M.; Fang, Z.; Chen, W. *J Membr Biol* **2014,** 247, (7), 601-9.

30. Rodland, K. D.; Bollinger, N.; Ippolito, D.; Opresko, L. K.; Coffey, R. J.; Zangar, R.; Wiley, H. S. *J Biol Chem* **2008,** 283, (46), 31477-87.
31. McLaughlin, S.; Smith, S. O.; Hayman, M. J.; Murray, D. *J Gen Physiol* **2005,** 126, (1), 41-53.
32. Taghian, T.; Narmoneva, D. A.; Kogan, A. B. *J R Soc Interface* **2015,** 12, (107).
33. Levin, M.; Stevenson, C. G. *Annual review of biomedical engineering* **2012,** 14, 295-323.

Figure Captions.

Figure 1. The reporter cell and chip design. (a) A schematic of ERK translocation reporter (ERKTR, pink color) translocate from the nucleus to cytosol upon activation of EGFR-Ras-ERK signaling pathway. (b) Left: The overall of the microelectrode arrays on the glass cover slip. Right: An optical image of one pair of microelectrodes at the center of the chip. The white arrows mark the metal connections that are passivated by 500 nm thick SU-8 polymer. The black arrows mark the exposed parallel microelectrodes. Scale bars, left: 5 mm, right: 200 μm. (c) The waveform of the bipolar electric pulses applied to the electrodes. (d) Left: A photo of the assembled cell chamber on the chip and printed circuit board (PCB). Scale bar 10 mm. The yellow dash line marks the position of the cross-section shown on the right. Right: Schematics of the cross-section structure of the chamber.

Figure 2. Localized ERK activation by AC EF. (a) AC EF induced localized ERK activation between a pair of microelectrode bars (marked by the arrows). (b-c) Cells between the microelectrodes (b) and in an adjacent area (c) before and after onset of stimulation. The color-coded images on the right of each panel show the difference of fluorescence intensity before and after stimulation. Blue and orange colors mark areas where the fluorescence intensity decrease and increase respectively. (d) Time traces of ERKTR ratio of individual representative cells and population average from 164 cells within 100 μm from the electrode. Average data are presented as mean (thick blue line) ± SD (light shadow). Black arrow denotes the time of applying AC-EF and red line indicate the sustained EF stimuli. (e) Time traces of ERKTR ratio of individual representative cells and population average from 160 cells within the region of 200 to 700 μm away from the electrode. Data are presented as mean (thick blue line) ± SD (light shadow). Black arrow denotes the time of applying AC-EF and red line indicate the sustained EF stimuli.

Figure 3. ERK oscillations under sustained AC EF stimulation. (a) Three cells showing oscillation of ERK under continuous AC EF stimulation. Fluorescent images taken at 0, 10, 20, 30, 40, 50 and 60 minute as continuous AC EF stimuli were applied. Cells circled in orange, blue, and green all demonstrated repeated pulsatile ERK activation. Scale bar: 20 μm. (b) Time traces of the ERKTR ratio of the three cells in (a**)**, peaks (ERK active) and valleys (ERK at rest) were identified. The black arrow denotes the start time of EF stimulation and red line marks the sustained EF stimuli. (c) Peak time map of the 164 cells in Fig. 2D under sustained AC EF stimulation. 35 cells showed multiple peaks (>=2) in 3 hours. The black dashed line indicated the time of exposure to AC EF stimulation.

Figure 4. Repeated short AC-EF stimulation induced synchronized ERK activation. (a) Fluorescent images of cells before (left) and after (middle) the 3-minute long AC EF stimulations started at 0, 48 and 93 min. Right: Color coded intensity difference. Blue and orange colors mark areas where the fluorescence intensity decreased and increased, respectively. Scale bar: 50 μm. (b) Time traces of ERKTR ratio from individual representative cells and population average from 17 cells. The short red lines mark the duration of EF stimuli. Data are presented as mean (thick blue line) **±** SD (light shadow). (c) Peak time map of ERK activities.

Figure 5. Blocker tests following the EGFR-Raf-ERK signaling pathway. (a) Schematics of the EGF-Ras-ERK signaling pathway and the blocked sites, including the extracellular EGF binding site, the intracellular phosphorylation site of EGFR, Raf and MEK. (b-h) (Images on the left group) Fluorescence images of cells before and after AC EF stimulation, and the intensity difference; and (Images on the right group) fluorescence images of control groups stimulated by EGF chemical stimulation (2ng/mL), when no inhibitors were applied (b), and with MEK inhibitor trametinib (0.5 μM) (c), Raf inhibitor sorafenib (20 μM) (d), tyrosine kinase inhibitors afatinib (5 μM) (e), erlotinib (2 μM) (f), gefitinib (50 μM) (g), and EGFR binding-site antibody cetuximab (100 μg/mL) (h), respectively. Scale bars: 25 μm. (i) Time traces of ERKTR ratio as population average from cells under AC EF

stimulations in (b-h). Mean and ± 95%CI are shown as a solid line and shadow region, respectively (n > 100 cells for each group).

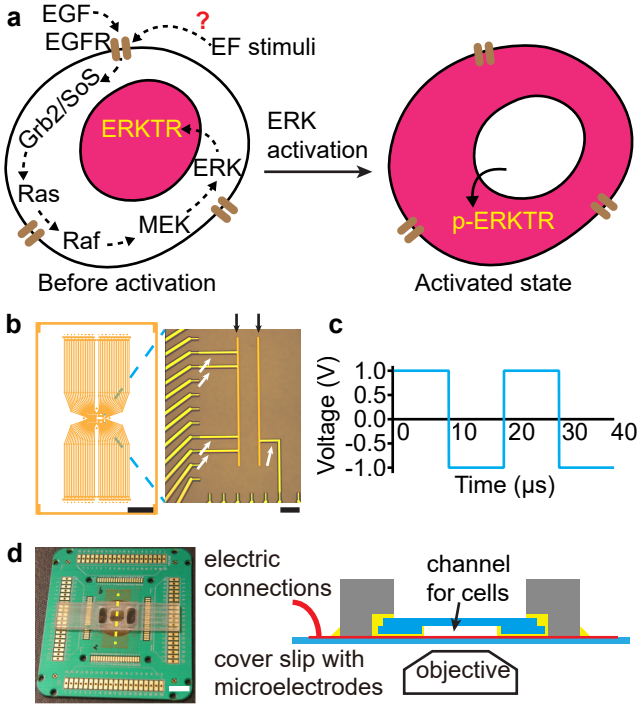
a
EGF
EGFR
?
EF stimuli
Grb2/SoS
ERKTR
ERK
Ras
Raf
MEK
Before activation
ERK
activation
p-ERKTR
Activated state
b
c
Voltage (V)
1.0
0.5
0.0
-0.5
-1.0
0
10
20
30
40
Time (μs)
d
electric
connections
channel
for cells
cover slip with
microelectrodes
objective

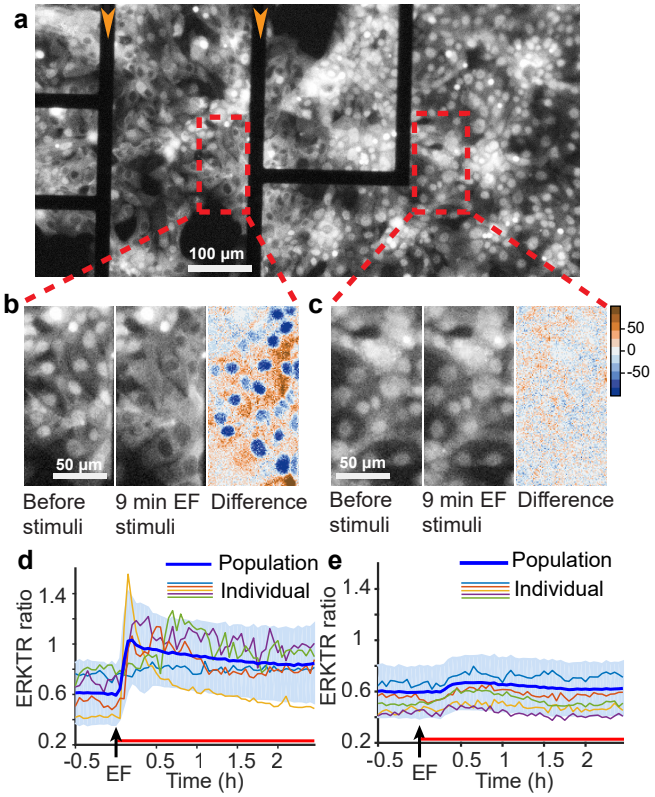
a
100 μm
b
c
50
0
-50
50 μm
50 μm
Before stimuli
9 min EF stimuli
Difference
Before stimuli
9 min EF stimuli
Difference
d
Population
Individual
ERKTR ratio
1.4
1
0.6
0.2
-0.5
EF
0.5
1
1.5
2
Time (h)
e
Population
Individual
ERKTR ratio
1.4
1
0.6
0.2
-0.5
EF
0.5
1
1.5
2
Time (h)

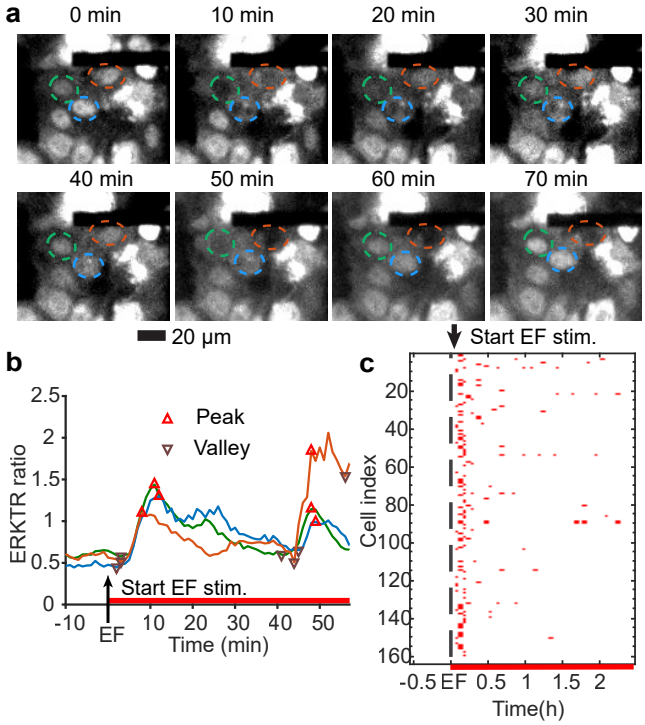
a
0 min
10 min
20 min
30 min
40 min
50 min
60 min
70 min
20 μm
b
Peak
Valley
ERKTR ratio
Start EF stim.
EF
Time (min)
c
Start EF stim.
Cell index
EF
Time(h)

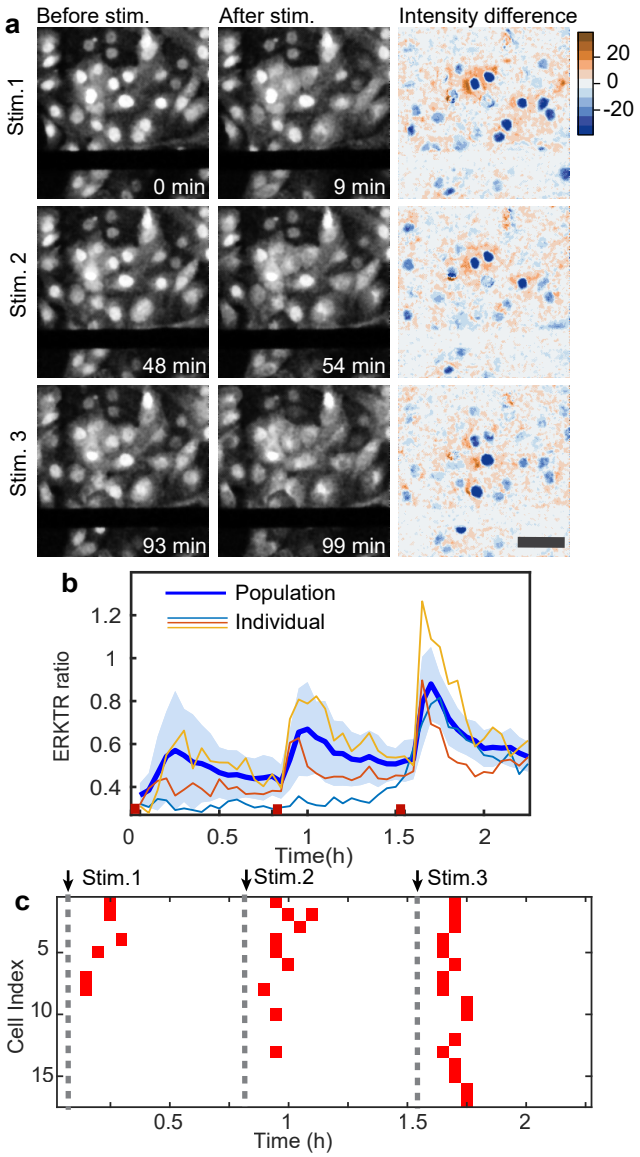
a
Before stim.
After stim.
Intensity difference
Stim.1
Stim. 2
Stim. 3
0 min
9 min
48 min
54 min
93 min
99 min
20
0
-20
b
Population
Individual
ERKTR ratio
1.2
1
0.8
0.6
0.4
0
0.5
1
1.5
2
Time(h)
c
Stim.1
Stim.2
Stim.3
Cell Index
5
10
15
0.5
1
1.5
2
Time (h)

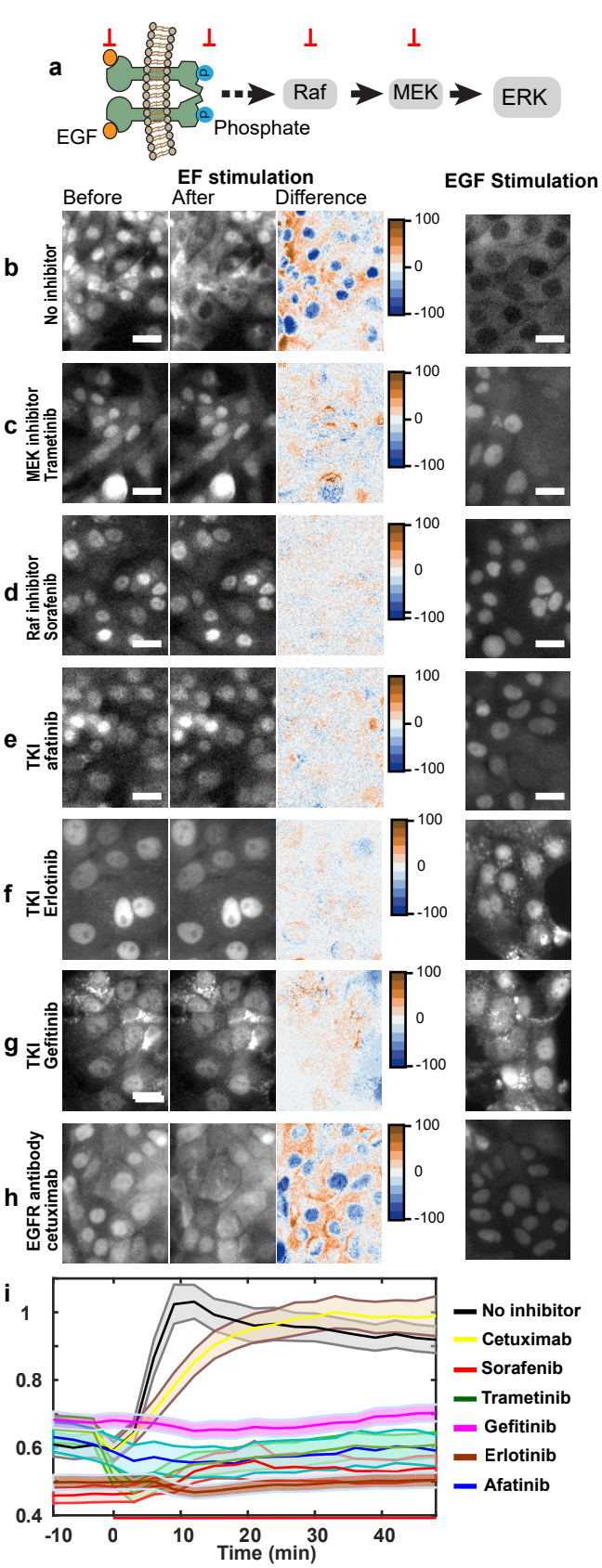
a
EGF
Phosphate
Raf
MEK
ERK
EF stimulation
Before
After
Difference
EGF Stimulation
b
No inhibitor
c
MEK inhibitor Trametinib
d
Raf inhibitor Sorafenib
e
TKI afatinib
f
TKI Erlotinib
g
TKI Gefitinib
h
EGFR antibody cetuximab
100
0
-100
i
1
0.8
0.6
0.4
-10
0
10
20
30
40
Time (min)
No inhibitor
Cetuximab
Sorafenib
Trametinib
Gefitinib
Erlotinib
Afatinib

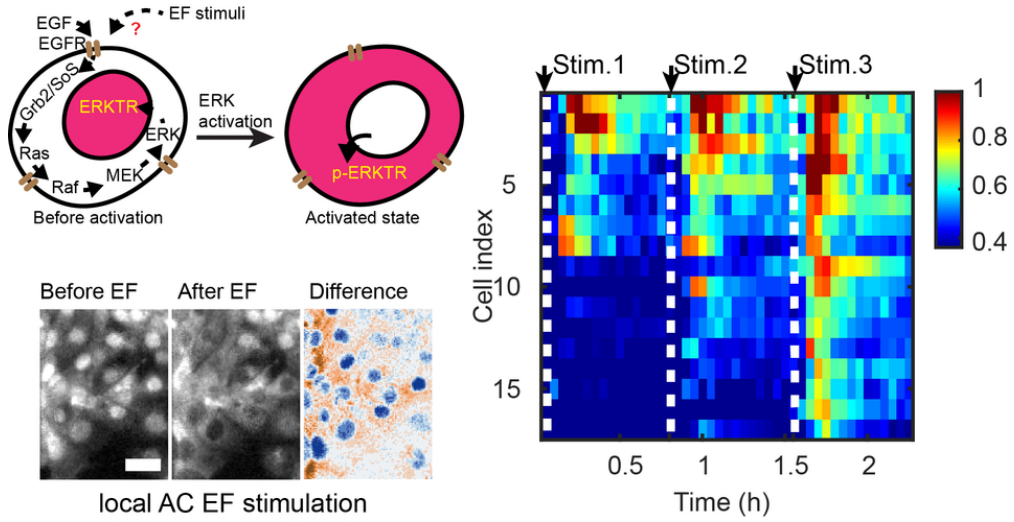

80x41mm (300 x 300 DPI)